Received: 23 October 2018 | Revised: 30 March 2019 | Accepted: 3 April 2019

DOI: 10.1002/ardp.201800310

FULL PAPER

DPhG ARCH PHARM Archiv der Pharmazie

Synthesis of 2-(2-oxo-2*H*-chromen-4-yl)acetamides as potent acetylcholinesterase inhibitors and molecular insights into binding interactions

Jiraporn Kara[1] | Paptawan Suwanhom[1] | Chatchai Wattanapiromsakul[2] | Teerapat Nualnoi[3] | Jindaporn Puripattanavong[2] | Pasarat Khongkow[4] | Vannajan Sanghiran Lee[5] | Anand Gaurav[6] | Luelak Lomlim[1]

[1]Department of Pharmaceutical Chemistry, Faculty of Pharmaceutical Sciences, Prince of Songkla University, Hat Yai, Songkhla, Thailand

[2]Department of Pharmacognosy and Pharmaceutical Botany, Faculty of Pharmaceutical Sciences, Prince of Songkla University, Songkhla, Thailand

[3]Department of Pharmaceutical Technology, Faculty of Pharmaceutical Sciences, Prince of Songkla University, Hat Yai, Songkhla, Thailand

[4]Faculty of Medicine, Institute of Biomedical Engineering, Prince of Songkla University, Songkhla, Thailand

[5]Department of Chemistry, Faculty of Science, University of Malaya, Kuala Lumpur, Malaysia

[6]Department of Pharmaceutical Chemistry, Faculty of Pharmaceutical Sciences, UCSI University, Kuala Lumpur, Malaysia

Correspondence
Luelak Lomlim, Department of Pharmaceutical Chemistry, Faculty of Pharmaceutical Sciences, Prince of Songkla University, 15 Karnjanavanich Rd., Hat Yai, Songkhla 90112, Thailand.
Email: luelak.l@psu.ac.th

Funding information
Prince of Songkla University, Grant/Award Number: PHA570404S; University of Malaya, Grant/Award Numbers: RP020C-14AFR, GPF063B-2018

Abstract

Sixteen novel coumarin-based compounds are reported as potent acetylcholinesterase (AChE) inhibitors. The most active compound in this series, **5a** (IC_{50} 0.04 ± 0.01 μM), noncompetitively inhibited AChE with a higher potency than tacrine and galantamine. Compounds **5d**, **5j**, and **5 m** showed a moderate antilipid peroxidation activity. The compounds showed cytotoxicity in the same range as the standard drugs in HEK-293 cells. Molecular docking demonstrated that **5a** acted as a dual binding site inhibitor. The coumarin moiety occupied the peripheral anionic site and showed π-π interaction with Trp278. The tertiary amino group displayed significant cation-π interaction with Phe329. The aromatic group showed π-π interaction with Trp83 at the catalytic anionic site. The long chain of methylene lay along the gorge interacting with Phe330 via hydrophobic interaction. Molecular docking was applied to postulate the selectivity toward AChE of **5a** in comparison with donepezil and tacrine. Structural insights into the selectivity of the coumarin derivatives toward *hu*AChE were explored by molecular docking and 3D QSAR and molecular dynamics simulation for 20 ns. ADMET analysis suggested that the 2-(2-oxo-2*H*-chromen-4-yl)acetamides showed a good pharmacokinetic profile and no hepatotoxicity. These coumarin derivatives showed high potential for further development as anti-Alzheimer agents.

KEYWORDS
3D QSAR, acetylcholinesterase inhibitor, coumarin, lipid peroxidation, molecular docking

1 | INTRODUCTION

Alzheimer's disease (AD) is the most common form of dementia. The symptoms start with difficulty in remembering new information and recent events, followed by apathy, depression, subsequent impaired judgment, confusion, and behavior change. Etiology of AD is complicated and still unclear. β-Amyloid aggregation and neurofibrillary tangles are major abnormalities found in the brain of patients with AD, which eventually lead to neuronal damage. This results in the decrease of acetylcholine (ACh), the neurotransmitter responsible for memory and learning. Acetylcholinesterase inhibitors (AChEIs), such as tacrine, donepezil, galantamine, and rivastigmine,

are the major drugs prescribed for patients with AD. These agents reversibly inhibit acetylcholinesterase that degrades ACh, and in turn increase the ACh level in the brain.[1]

AChEIs have been used in clinics for several decades. However, the 3D structure of the enzyme was unknown until the 1990s when the crystal structure of *Torpedo californica* AChE was first reported.[2] It has been found that the active site of AChE appears as a deep and narrow gorge with aromatic amino acid residues lining the entrance of the gorge forming the peripheral anionic site (PAS). The catalytic anionic site (CAS) is located underneath the PAS. This is the area where Trp84 binds to the ammonium group of ACh and, subsequently, the acetyl group of ACh orientated to the the acetylation site (Ser200) at the bottom of the gorge. Hydrolysis of ACh by the Ser200 residue then occurs, resulting in acetylated Ser200 residue (inactive AChE) and choline as products.

Butyrylcholinesterase (BChE) is another enzyme that hydrolyzes ACh. Both cholinesterase enzymes differ in substrate specificity, enzyme kinetics, expression and activity in different brain regions. In a normal brain, the activity of BChE is relatively low but progressively increases as AD advances while AChE activity declines. Therefore, inhibition of BChE may provide an additional benefit in AD treatment.[3] BChE contains 524 amino acids. The active site of the enzyme is similar to AChE.[4] AChEI molecules vary in their selectivity for AChE vs BChE. Tacrine and galantamine mainly bind with the CAS and inhibit AChE and BChE with close IC_{50} values.[5] Donepezil binds with both CAS and PAS, acting as a dual binding site inhibitor and showing higher selectivity toward AChE.[6,7]

The coumarin ring has been of high interest as a scaffold for design of several potent AChEIs.[8–24] In previous studies, coumarin moiety showed affinity to the PAS of AChE due to its aromatic character that facilitates the π-π interaction with the amino acid residues in the region. Amino group-containing moiety of the compounds occupied the CAS of the active site gorge showing cation-π interaction. Although most reported coumarin derivatives were substituted with amino group-containing moiety on position 3 or 7 of the coumarin ring system, potent AChEIs with phenyl piperazinyl moiety substituted on position 4 of the coumarin ring were also reported.[9,14] Recently, isoindoline-1,3-dione and related derivatives of 1-benzylpiperazine, which were developed by our group and others, showed relatively high acetylcholinesterase inhibitory activity and the benzyl-piperazinyl moiety was suggested to be responsible for interaction with CAS.[25–27] In this study, coumarin derivatives with *N*-substituted benzylpiperazinyl moiety replaced on position 4 of the coumarin ring were designed as shown in Figure 1.

Research proposes that oxidative stress plays a role in initiating β-amyloid aggregation and tau protein hyperphosphorylation.[28–31] Thus, prevention of oxidative stress-induced neuronal cell damage has become another approach to AD therapy. The antioxidative activity of numerous coumarin derivatives has been reported.[16,19] Therefore, the lipid peroxidation inhibitory effects of the designed compounds have also been investigated.

Furthermore, the synthesized compounds were evaluated for their cytotoxicity. An enzyme kinetic study was performed with the most active compound to determine the mode of AChE inhibition. Insights in binding interaction between the coumarin derivative and AChE and BChE were predicted by molecular docking and atom-based 3D-QSAR. Drug-likeness properties of compounds in this series were anticipated via ADMET analysis. The molecular dynamics simulations were performed on the selected compound to confirm the stability in the binding pockets.

2 | RESULTS

2.1 | Acetyl- and butyrylcholinesterase inhibitory activities

Acetyl- and butyrylcholinesterase inhibitory activities of the synthesized compounds were evaluated by comparing to the drugs donepezil, tacrine, and galantamine (Table 1). Compound **5a** (IC_{50} = 0.04 μM, *hu*AChE) was the most potent AChEI in this series. The compound exhibited inhibitory activity against AChE in the micromolar scale (0.04-27 μM) and showed a higher potency than tacrine (IC_{50} = 0.10 μM) and galantamine (IC_{50} = 0.75 μM). The selectivity index (SI) of the coumarins ranged from 0.06 to 17.

2.2 | Kinetic study

Compound **5a** was chosen as a representative for this assay because it shows the highest AChE inhibitory activity. Model fittings for evaluating the mode of inhibition were carried out with a global nonlinear regression mode of the GraphPad Prism software and are presented in a double reciprocal Lineweaver-Burk plot (Figure 2).

2.3 | Antilipid peroxidation activity

As shown in Table 1, compounds **5d**, **5j**, and **5 m** showed a moderate antioxidant activity while other compounds exhibited only weak antilipid peroxidation activity.

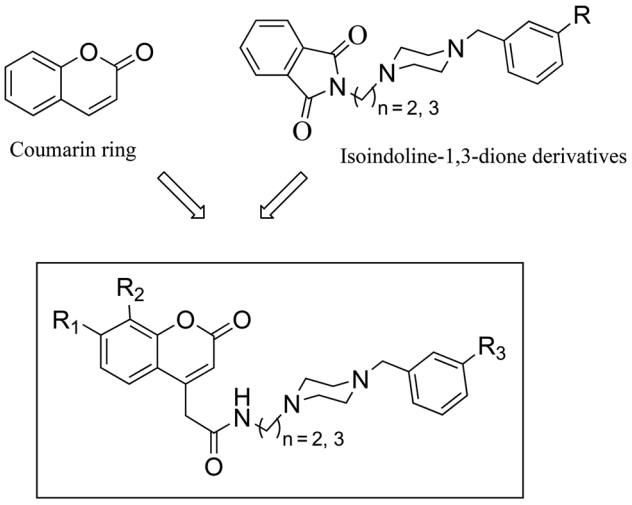

FIGURE 1 Design of coumarin derivatives

TABLE 1 Inhibitory activity against AChE and BChE, antilipid peroxidation and in vitro cytotoxic activities of the synthesized derivatives against HEK-293 cell lines

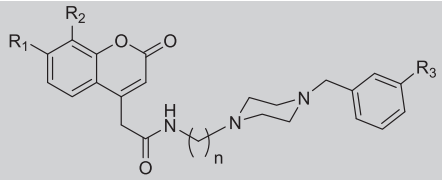

Cpd.	R_1	R_2	R_3	n	IC_{50} (μM ± SEM) *hu*AChE[a]	IC_{50} (μM ± SEM) *hu*BChE[b]	SI[c]	Linoleic acid peroxidation inhibition assay[d] % inhibition ± SD	Cytotoxicity LC_{50} (μM)
5a	OH	CH_3	H	2	0.04 ± 0.01	0.68 ± 0.07	17	25.18 ± 0.06	56.388
5b	OH	CH_3	F	2	1.33 ± 0.21	1.30 ± 0.12	0.98	5.76 ± 0.05	62.921
5c	OH	CH_3	CH_3	2	9.05 ± 0.49	1.94 ± 0.25	0.21	42.52 ± 0.04	85.621
5d	OH	CH_3	NO_2	2	26.09 ± 0.44	1.52 ± 0.19	0.06	65.60 ± 0.01	67.545
5e	OH	CH_3	H	3	7.02 ± 0.06	14.62 ± 0.85	2.08	29.57 ± 0.01	57.108
5f	OH	CH_3	F	3	2.92 ± 0.20	17.63 ± 0.62	6.04	32.45 ± 0.01	>100
5g	OH	CH_3	CH_3	3	12.94 ± 0.44	11.61 ± 0.58	0.90	n.d.	n.d.
5h	OH	CH_3	NO_2	3	9.45 ± 0.27	19.61 ± 1.06	2.08	n.d.	n.d.
5i	OCH_3	H	H	2	0.43 ± 0.03	2.72 ± 0.14	6.33	23.74 ± 0.04	76.701
5j	OCH_3	H	F	2	16.56 ± 0.40	17.24 ± 0.27	1.04	55.81 ± 0.03	86.454
5k	OCH_3	H	CH_3	2	1.20 ± 0.03	5.05 ± 0.33	4.21	34.60 ± 0.02	>100
5l	OCH_3	H	NO_2	2	5.23 ± 0.13	68.44 ± 2.66	13.09	39.64 ± 0.04	>100
5m	OCH_3	H	H	3	3.47 ± 0.12	19.03±0.91	5.48	50.10 ± 0.07	70.131
5n	OCH_3	H	F	3	10.46 ± 0.70	23.49 ± 1.74	2.25	n.d.	n.d.
5o	OCH_3	H	CH_3	3	12.61 ± 0.32	21.22 ± 0.58	1.68	42.45 ± 0.01	>100
5p	OCH_3	H	NO_2	3	27.29 ± 1.16	11.55 ± 0.73	0.42	43.24 ± 0.04	82.146
Donepezil					0.004 ± 0.0001	1.90 ± 0.02	475	n.d.	69.751
Tacrine					0.10 ± 0.003	0.02 ± 0.003	0.2	n.d.	72.247
Galantamine					0.75 ± 0.03	2.70 ± 0.09	3.6	n.d.	83.182
BHT					…	…	…	95.11 ± 0.04	n.d.

Note. BHT: butylated hydroxytoluene; nd: not determined; SD: standard deviation; SEM: standard error of mean.
[a]human acetylcholinesterase.
[b]human butyrylcholinestrase.
[c]SI = selectivity index = IC_{50}BChE/IC_{50}AChE.
[d]Data are reported as mean ± standard deviation (n = 3).

2.4 | Cytotoxicity assessment

The results from the SRB assay are shown in Table 1. Generally, all of the tested compounds displayed low cytotoxicity (LC_{50} > 50 μM). Compound **5a**, the most potent acetylcholinesterase inhibitor in this series, showed LC_{50} at 56.388 μM. This value is more than 1000-fold higher than the concentration for human AChE inhibition.

2.5 | Molecular docking and molecular dynamics simulations

Several conformers of structure with favorable binding affinity as indicated by the low negative values in the range from −11.9 to −7.8 kcal/mol (Table 2) were retrieved. Compound **5a** was analyzed in comparison to donepezil. Donepezil (binding energy −11.9 kcal/mol) was bound with *hu*AChE with a slightly higher affinity than **5a** (binding energy −11.6 kcal/mol). This result corresponded with the findings in the enzyme inhibition assay. The structures of the donepezil, tacrine, and **5a** complexes were minimized and the residue interaction energy with *hu*AChE and *hu*BChE in 4 Å region from the ligands are reported in Table 3. The docking model of donepezil, **5a** and tacrine with *hu*AChE and *hu*BChE are illustrated in Figure 3. Compound **5a** was stably bound in the binding pocket throughout 20 ns MDs. The complexed structure at 20 ns, potential energy and the root mean square displacement data are reported in the Supporting Information.

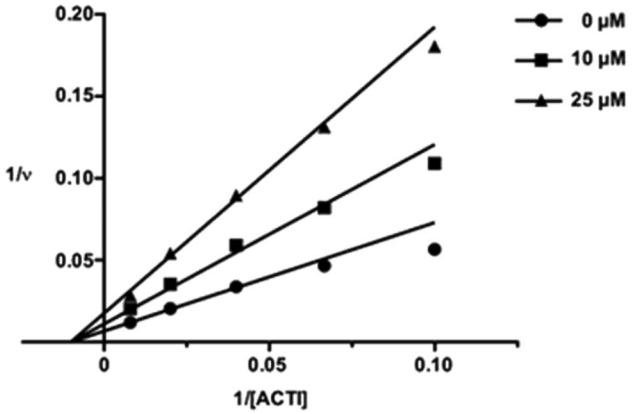

FIGURE 2 Kinetic assay for AChE inhibition by **5a.** The kinetic assay of AChE inhibition was carried out at 0, 10, and 25 μM of compound **5a**. The concentration of ATCI substrate was varied between 10 to 125 μM. The resulting over-layered double reciprocal Lineweaver-Burk plot generated by the GraphPad Prism software demonstrated that compound **5a** inhibited the enzyme by noncompetitive mode

2.6 | 3D QSAR

The atom-based 3D QSAR model was built using the 3D QSAR model module of Discovery Studio 3.1. Default settings were used for model development. Validation of the developed model was performed based on the internal predictions of the data set and leave-one-out cross-validation method (five-fold). PLS analyses of the data sets using three principal components showed a high cross-validated r^2_{cv} value of 0.788, RMS residual error (cross-validation) of 0.311, noncross-validated r^2 value of 0.898, RMS residual error of 0.201, r^2adj of 0.873. pIC_{50} values of the synthesized compounds for *hu*AChE and *hu*BChE and the AChE selectivity index (SI) are listed in Supporting Information. In a plot of actual vs predicted SI, predicted value was obtained using the developed 3D QSAR model. the van der Waals and electrostatic contour plots were obtained using the atom based 3D QSAR methods.

2.7 | ADMET analysis

All compounds conformed to Lipinski's rule of five (MW < 500; AlogP < 5; donorHB ≤ 5; acceptorHB ≤ 10) (see Supporting Information).

3 | DISCUSSION

3.1 | Acetyl- and butyrylcholinesterase inhibitory activities

Cholinesterase inhibitory activity of the synthesized compounds is shown in Table 1. Among 7-hydroxyl-8-methyl coumarin derivatives with ethylene linker (n = 2) (**5a**–**d**), the most potent *hu*AChE inhibitor in this series was **5a** (0.04 ± 0.01 μM). Substitution on 3-position of the benzyl moiety with F, CH_3, and NO_2 groups led to decreased activity. While clear electron donating/withdrawing effects of the substituents on the inhibitory activity was not observed, the larger size of the substituents seemed to reduce activity. When the ethylene linker was changed to propylene linker (n = 3) (**5e**–**h**), the corresponding derivatives showed lower potency, with the exception of **5h** which exerted higher potency than **5d**.

For 7-methoxyl coumarin derivatives with ethylene linker (n = 2) (**5i**–**l**), substitution on R_3 also decreased huAChE inhibitory activity. An increase in size of the substituent resulted in a more potent inhibitor. An extension of the linker to propylene group resulted in increased activity of the corresponding derivatives (**5m**–**p**) with the exception of **5n**. Substitution on 3-position of the benzyl moiety of 7-hydroxyl-8-methyl coumarin derivatives with ethylene linker (n = 2) (**5a**–**d**) resulted in a slight decrease in BChE inhibitory activity. Change from ethylene linker to propylene linker led to reduced activity (**5e**–**h**). The same trend was observed in the 7-methoxyl coumarin series. Additionally, all the compounds evaluated in this study showed no selectivity toward AChE as indicated by the low selectivity index (SI).

3.2 | Kinetic study

Kinetic analysis of AChE inhibition was performed to determine the inhibition mode of the compounds in this series. In the Lineweaver-Burk plot (Figure 2), V_{max} decreased but K_m was not affected as the increase of concentration of the inhibitor. The result suggested that compound **5a** is a noncompetitive inhibitor with an inhibition constant (K_i) of 15.29 μM.

3.3 | Antilipid peroxidation activity

Since the brain tissues are rich in phospholipids, free-radical induced lipid peroxidation can be another factor that causes brain damage. Several synthetic and natural coumarin derivatives have potential antioxidant activity.[16,19,32–34] The compounds in this series showed only low to moderate anti-lipid peroxidation activity in comparison to butylated hydroxytoluene (BHT).

3.4 | Cytotoxicity assessment

Selected compounds in this series were evaluated for their cytotoxicity against human embryonic kidney (HEK-293) cells compared with the reference drugs. HEK-293 has characteristics of immature neurons and is used in neuroscience research. **5a** showed LC_{50} at 56.388 μM (Table 1). This value is more than 1000-fold higher than the concentration for human AChE inhibition.

3.5 | Molecular docking and molecular dynamics simulations

The binding mode between the commercial drugs (donepezil and tacrine) and **5a** were compared. Two docking centers were set at the center of the PAS and CAS binding sites. The *hu*AChE and the *hu*BChE crystal structures have very high similarity of amino acid

TABLE 2 Binding affinity in kcal/mol from AutoDock Vina. The structures in mode A are in the same direction as the binding mode of the drugs in the X-ray structure (-benzyl in donepezil toward the inner gorge and -NH_2 in tacrine lied in the same side as in X-ray) whereas those in mode B are also the low energy structure but aligning in the opposite direction. The docked structures of ligands are in a ball and stick model; nonpolar hydrogens are not shown and the line structures of donepezil and tacrine from the X-ray structure are superposed in blue and green.

Compounds	IC_{50} (μM ± SEM) *hu*AChE / *hu*BChE	Binding affinity (kcal/mol) *hu*AChE PAS	*hu*AChE CAS	*hu*BChE PAS	*hu*BChE CAS
Donepezil 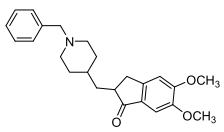	0.004 ± 0.0001 / 1.90 ± 0.02	A) −11.9 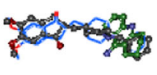 B) −10.0 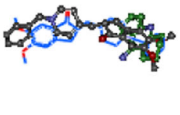	A) −11.0 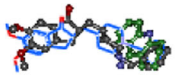 B) −11.9 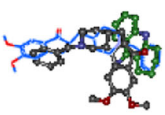	A) −9.5 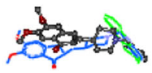 B) −9.8 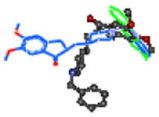	A) −9.8 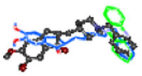 B) −9.4 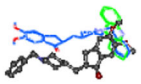
Tacrine 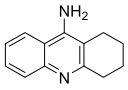	0.10 ± 0.003 / 0.02 ± 0.003	A) −8.7 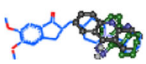 B) −8.7 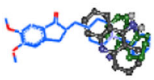	A) −8.7 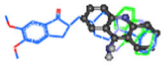 B) −8.7 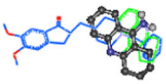	A) −8.0  B) −7.9 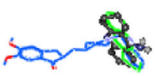	A) −8.0 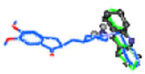 B) −7.8 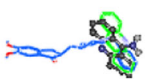
5a 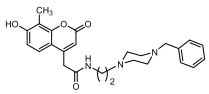	0.04 ± 0.01/ 0.68 ± 0.07	A) −11.6 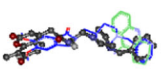 B) −11.9 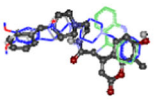	A) −10.3 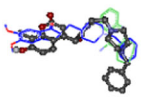 B) −11.3 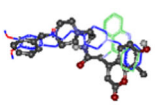	A) −10.4 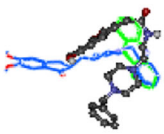 B) −10.5 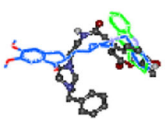	A) −10.4 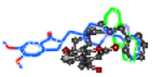 B) −10.4 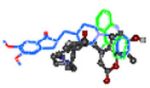

sequence homology with similar molecular forms and active center structure; however, the binding cavity volume for the *hu*AChE is larger to accommodate donepezil (about 347.63 $Å^3$), whereas the *hu*BChE is about 246.75 $Å^3$ in binding with tacrine.

From IC_{50} values, donepezil is specific and preferably bound to a larger cavity of *hu*AChE than *hu*BChE whereas tacrine, which has a smaller size, can bind to both structures. Compound **5a** is similar in structure to donepezil; however, a slight reduction of the binding affinity from −11.9 to −11.6 kcal/mol in the PAS pocket was observed, reflecting the lower selectivity of **5a** against AChE compared to donepezil. The selectivity index (IC_{50} BChE/ IC_{50} AChE) has shifted from 475 (donepezil) to 17 (**5a**). **5a** had slightly better activity for *hu*AChE than tacrine; however, tacrine had the best affinity to *hu*BChE among all the compounds. The AutoDock Vina results correlated well with the *hu*AChE activity results where the best binding of donepezil > **5a** > tacrine was found, but the correlation was not in agreement with *hu*BChE which theoretically indicated better binding affinity of **5a** than tacrine where the experimental result observed better activity of tacrine > **5a** > donepezil. **5a** fit well in the AChE pocket and due to its large molecular size, could not fit into the BChE cavity and ended up with a curl structure (Table 2). The residue interaction at the binding

TABLE 3 Contribution of van der Waals (VDW) and electrostatic (Elect) interaction energy (IE, kcal/mol) of *hu*AChE and *hu*BChE residues in 4 Å region from donepezil, tacrine, and **5a**. The residues in the inner gorge are in bold

	Donepezil				Tacrine				5a		
Residue	IE	VDW	Elect	Residue	IE	VDW	Elect	Residue	IE	VDW	Elect
*hu*AChE residues											
A_TYR72	1.26	−2.33	3.59	A_ASP74	−2.02	−1.1	−0.92	A_TYR72	−1.53	−1.78	0.25
A_ASP74	−4.34	−2.55	−1.79	A_TRP86	−5.41	−4.6	−0.82	A_ASP74	−6.85	−2.23	−4.62
A_THR83	1.33	−0.5	1.83	A_TYR119	−2.79	−0.35	−2.44	A_THR83	1.2	−0.48	1.68
A_TRP86	−3.06	−4.57	1.51	A_GLY120	−2.02	−2.25	0.23	**A_TRP86**	−0.36	−4.95	4.6
A_GLY120	−1.15	−1.21	0.06	A_GLY121	−2.36	−1.82	−0.54	**A_GLY120**	−0.96	−1.43	0.47
A_GLY121	−3.35	−1.19	−2.16	A_TYR124	−1.28	−1.1	−0.18	**A_GLY121**	−8.59	−1.39	−7.19
A_TYR124	−4.24	−2.71	−1.53	A_SER125	−0.09	−0.52	0.43	A_TYR124	5.06	−3.39	8.46
A_TYR133	−0.75	−0.5	−0.25	A_TYR133	2.25	−1.01	3.26	**A_TYR133**	0.99	−0.57	1.56
A_GLU202	−3.66	−1.16	−2.5	A_GLU202	−2.1	−1.33	−0.77	**A_GLU202**	−4.55	−1.26	−3.29
A_SER203	−3.74	−0.75	−2.99	A_SER203	−5.07	−1.24	−3.83	**A_SER203**	−1.94	−0.65	−1.29
A_TRP286	−5.43	−5.72	0.29	A_TYR337	−3.96	−3.08	−0.88	A_TRP286	−8.47	−7.91	−0.56
A_LEU289	0.79	−0.39	1.19	A_PHE338	−1.15	−2.23	1.08	A_LEU289	−4.6	−1.69	−2.91
A_GLU292	8.43	−0.53	8.97	A_TYR341	−1.95	−1.73	−0.22	A_GLU292	3.25	−0.41	3.66
A_SER293	−6.26	−1.49	−4.77	A_HIS447	−7.82	−2.8	−5.02	A_SER293	1.03	−2.2	3.22
A_VAL294	−9.29	−2.18	−7.11	A_GLY448	0.07	−1.19	1.26	A_VAL294	−4.7	−1.64	−3.06
A_PHE295	−9.73	−1.26	−8.47	A_ILE451	3.32	−0.6	3.92	A_PHE295	2.05	−1.42	3.47
A_ARG296	−0.28	−0.58	0.3					A_ARG296	−2.37	−1.87	−0.5
A_PHE297	−1.09	−1.41	0.32					A_PHE297	−2.29	−2.85	0.56
A_TYR337	−3.56	−4.57	1.01					**A_TYR337**	−11.89	−4.18	−7.7
A_PHE338	−7.10	−4.42	−2.68					A_PHE338	−4.62	−3.32	−1.3
A_TYR341	−7.11	−7.96	0.86					A_TYR341	−8.02	−6.33	−1.69
A_GLY342	0.62	−0.37	0.99					**A_HIS447**	−0.86	−2.21	1.35
A_HIS447	−6.63	−2.63	−3.99					**A_GLY448**	−3.68	−0.85	−2.84
A_GLY448	−1.46	−1.03	−0.43					**A_ILE451**	−2.17	−0.65	−1.53
A_ILE451	−1.38	−0.35	−1.03								
IE in 4 Å	−71.17	−52.39	−18.78		−32.38	−26.94	−5.44		−64.85	−55.65	−9.2
IE inner	−28.74	−17.96	−10.77		−32.38	−26.94	−5.44		−34.01	−18.14	−15.86
IE	−72.76	−57.49	−15.27		−44.81	−30.95	−13.87		−85.41	−61.76	−23.66
*hu*BChE residues											
A_ASP70	−7.46	−2.81	−4.65	A_SER79	−1.27	−0.78	−0.49	A_ASP70	−6.19	−2.97	−3.22
A_SER72	−5.54	−0.79	−4.75	A_TRP82	−6.94	−7.28	0.34	A_GLY78	−1.38	−0.56	−0.82
A_SER79	0.96	−0.40	1.37	A_GLY115	−2.04	−1.54	−0.50	A_SER79	1.19	−2.18	3.37
A_TRP82	−3.95	−5.15	1.20	A_GLY116	−1.32	−1.27	−0.04	**A_TRP82**	−7.27	−6.07	−1.20
A_GLY115	−0.76	−1.63	0.87	A_THR120	0.01	−0.37	0.37	A_ASN83	−0.84	−0.70	−0.14
A_GLY116	−1.80	−1.55	−0.26	A_TYR128	1.23	−0.71	1.94	**A_GLY115**	−4.56	v2.30	−2.26
A_GLN119	−2.40	−1.61	−0.79	A_GLU197	−2.01	−1.41	−0.60	**A_GLY116**	−1.58	−4.39	2.82
A_THR120	1.63	−0.75	2.38	A_SER198	−2.79	−1.30	−1.49	A_GLY117	−6.52	−2.99	−3.53
A_TYR128	−2.21	−0.61	−1.60	A_ALA328	−1.34	−1.21	−0.13	A_THR120	3.46	−2.22	5.68
A_GLU197	8.98	−1.65	10.63	A_TYR332	−1.98	−1.34	−0.63	**A_TYR128**	−0.42	−0.70	0.29
A_SER198	−9.58	−1.50	−8.07	A_TRP430	−3.56	−1.63	−1.94	**A_GLU197**	0.85	−1.60	2.45
A_GLY283	−3.48	−0.48	−3.00	A_MET437	−0.26	−0.91	0.66	**A_SER198**	−0.69	−2.99	2.30
A_THR284	−3.91	−2.25	−1.65	A_HIS438	−5.04	−3.02	−2.02	A_TRP231	−0.51	−3.46	2.94
A_PRO285	−3.44	−4.75	1.31	A_GLY439	−1.32	−1.49	0.17	A_PRO285	−0.97	−0.99	0.02

(Continues)

TABLE 3 (Continued)

	Donepezil				Tacrine				5a		
Residue	**IE**	**VDW**	**Elect**	**Residue**	**IE**	**VDW**	**Elect**	**Residue**	**IE**	**VDW**	**Elect**
A_LEU286	−2.32	−1.58	−0.74	A_TYR440	−5.34	−1.40	−3.94	A_LEU286	−6.90	−4.34	−2.56
A_SER287	−2.41	−3.83	1.41	A_ILE442	−0.32	−0.33	0.01	A_SER287	4.72	−1.52	6.24
A_VAL288	−0.60	−0.57	−0.03					A_VAL288	−10.44	−1.77	−8.67
A_ASN289	−1.71	−0.70	−1.01					A_ALA328	−5.39	−0.94	−4.45
A_ALA328	−5.79	−1.00	−4.78					A_PHE329	−6.31	−5.10	−1.21
A_PHE329	−2.51	−2.60	0.09					A_TYR332	−3.21	−3.50	0.29
A_TYR332	−8.39	−4.64	−3.75					A_ASN397	−1.04	−0.37	−0.67
A_HIS438	−5.31	−3.23	−2.08					A_PHE398	−1.03	−1.66	0.63
A_GLY439	−1.80	−1.06	−0.74					A_TRP430	0.85	−0.53	1.38
A_ILE442	0.79	−0.32	1.11					**A_HIS438**	−5.23	−4.53	−0.70
								A_GLY439	−4.78	−1.70	−3.08
								A_TYR440	−8.01	−0.86	−7.14
								A_ILE442	−3.94	−1.02	−2.92
IE in 4 Å	−63.02	−45.49	−17.53		−34.29	−26.00	−8.29		−76.14	−61.97	−14.17
IE inner	−15.64	−16.69	1.05		−34.29	−26.00	−8.29		−27.62	−25.30	−2.30
IE	−52.00	−39.77	−12.23		−33.94	−23.81	−10.12		−59.36	−57.02	−2.34

Note. CAS for *hu*AChE: Ser203, Glu334, and His447; PAS for *hu*AChE: Tyr72, Asp74, Tyr124, Trp286; anionic site for *hu*AChE: Trp86. CAS for *hu*BChE: Ser198, Glu325 and His438; PAS for *hu*BChE: Tyr341 and Asp70 and Tyr332; anionic site for *hu*BChE: Trp82.

interface explained the activity of the compounds in agreement with the experimental investigation where the activity of donepezil (−71 kcal/mol) > **5a** (−65 kcal/mol) > tacrine (−32 kcal/mol). High affinity of tacrine toward *hu*AChE and *hu*BChE is from the interaction with inner gorge residues in the range of −32 to −34 kcal/mol, where donepezil and **5a** contributed to both inner and outer gorge.

The strong favorable interactions toward *hu*AChE (negative value, kcal/mol) are summarized in Table 3. For compound **5a**, *hu*AChE residues that showed interaction are Tyr337 (−11.89), Gly121 (−8.59), Trp286 (−8.47), Tyr341 (−8.02) and Asp74 (−6.85) while interaction energy of the inner gorge of enzyme (IE inner) are Trp86 (−0.36), Gly120 (−0.96), Gly121 (−8.59), Tyr133 (0.99), Glu202 (−4.05), Ser203 (−1.94), Tyr337 (−11.89), His447 (−0.86), Gly448 (−3.68) and Ile451 (−2.17) (IE inner = −34.01 kcal/mol). **5a** was able to bind both CAS and PAS of *hu*AChE. At the PAS, the coumarin ring interacted with the indole ring of Trp286 via π-π interaction (distance of 3.67 Å). At the mid-gorge, the long chain of methylene interacted with Phe338 and Tyr341 via the hydrophobic interaction. At the CAS, the benzyl group of compound can interact with π-π interaction by Trp86 (distance of 3.80 Å). These findings correspond with our rationale in designing the coumarin derivatives.

For *hu*BChE, the higher activity of tacrine > **5a** > donepezil can be explained in Table 3 where the interaction in the inner gorge was mainly interacting with the interaction energy (IE inner) of −34.29, −27.62, −15.64 kcal/mol. The favorable interaction toward *hu*BChE (-negative value) for donepezil are Ser198 (−9.58), Tyr332 (−8.39), Asp70 (−7.46), Ala328 (−5.79), Ser72 (−5.54) and His438 (−5.31) while the interaction of inner gorge of enzyme are Trp82 (−3.95), Gly115 (−0.76), Gly116 (−1.80), Tyr128 (−2.21), Glu197 (8.98), Ser198 (−9.58), His438 (−5.31), Gly439 (−1.80), Ile442 (0.79) (IE inner = −15.64 kcal/mol). Hydrophobic interaction with Tyr332 and Phe329 at midgorge of active site and π-π interaction between the benzyl group and Trp82 (distance of 3.82 Å) were exhibited.

Compound **5a** showed interaction via Val288 (−10.44), Tyr440 (−8.01), Trp82 (−7.27), Leu286 (−6.90), Gly117 (−6.52), Phe329 (−6.31), and Asp70 (−6.19) while interaction of the inner gorge of enzyme (IE inner) are Trp82 (−7.27), Gly115 (−4.56), Gly116 (−1.58), Tyr128 (−0.42), Glu197 (0.85), Ser198 (−0.69), His438 (−5.23), Gly439 (−4.78), Ile442 (−3.94) (IE inner = −27.62 kcal/mol). **5a** cannot fit into *hu*BChE cavity observed from the curl structure, but it can still interact with Tyr332 via the hydrophobic interaction and π-π interaction between the benzyl group and Trp82 (distance of 4.07 Å). Residues that showed interaction with tacrine were Trp82 (−6.94), Tyr440 (−5.34), His438 (−5.04). This compound bound only with CAS of the active site of enzyme as same as interaction with *hu*AChE (IE inner = −34.29 kcal/mol) and showed stacking interaction with Trp82 (distance of 3.59 Å) and Trp430 of the active site of *hu*BChE. Donepezil, **5a** and tacrine interactions with *hu*BChE are shown in Figure 3.

The docked structures of **5a** in binding with AChE and BChE were selected for MDs simulations. During the 20 ns MDs, **5a** remained stable inside the binding pocket of both enzymes. The MD final structure of **5a** inside AChE and BChE and potential energy and the RMSD of AChE and BChE with **5a** which indicated the stability of the complex are reported in the Supporting Information.

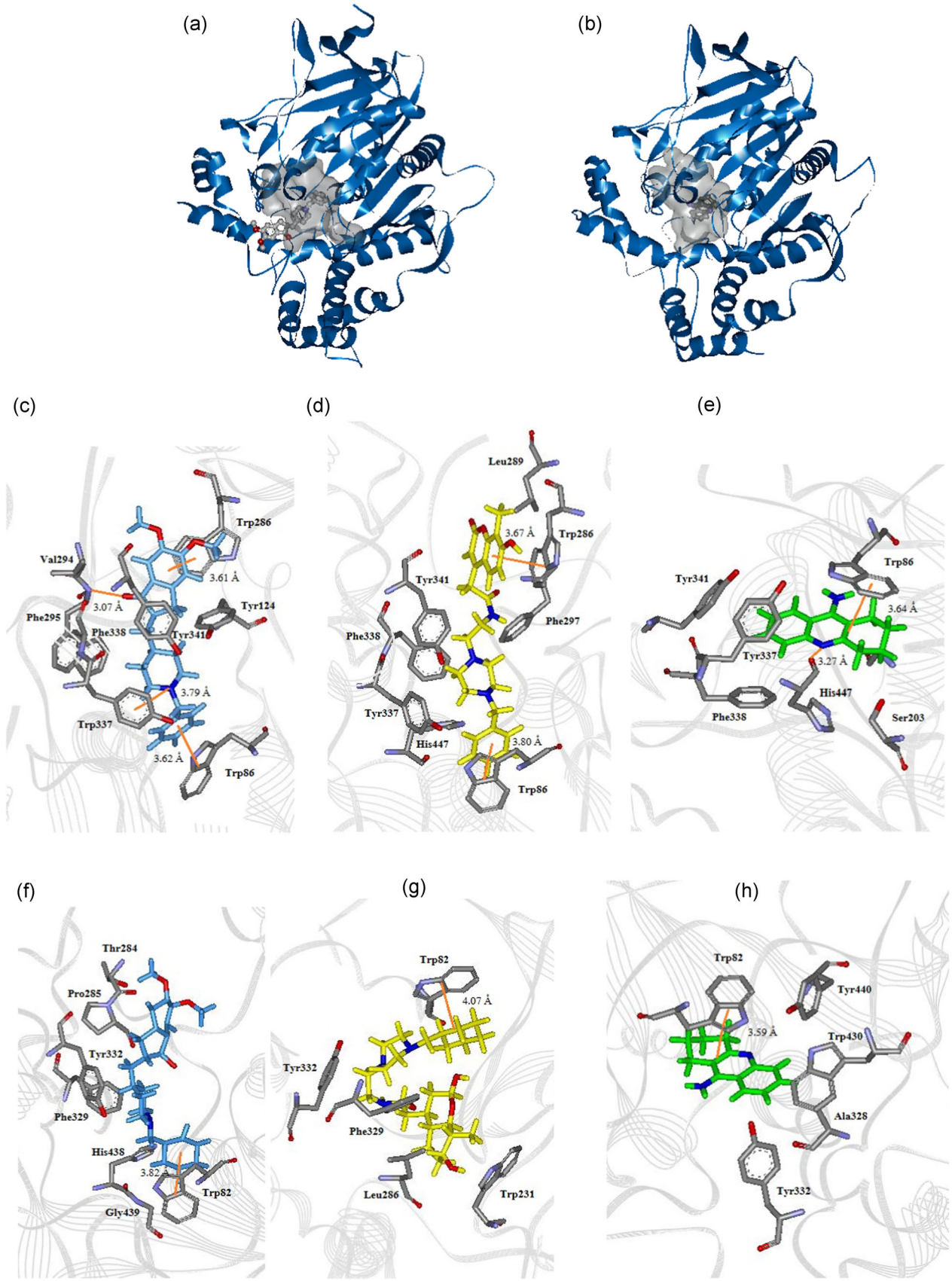

FIGURE 3 The crystal structure and the binding cavity (in gray) of *hu*AChE in complex with donepezil (a) and of *hu*BChE in complex with tacrine (b). Docking model of donepezil (c), **5a** (d) and tacrine (e)-*hu*AChE complex. Docking model of donepezil (f), **5a** (g), and tacrine (h)-*hu*BChE complex

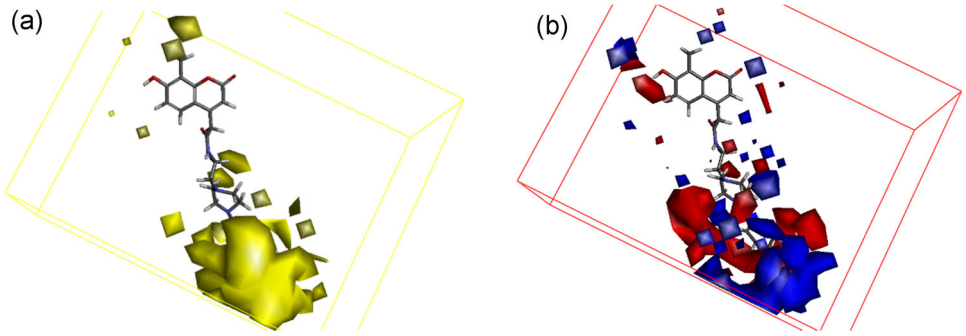

FIGURE 4 Compound **5a** mapped to (a) the van der Waals contour map; (b) the electrostatic contour map

3.6 | 3D QSAR

The atom-based 3D QSAR models were developed from the set of the 16 inhibitors using substructure based molecular overlay alignment. From the predicted *hu*AChE selectivity (SI) at 3rd PLS factor for the training and test set, it is quite evident that almost all compounds yielded a good predicted value (see Supporting Information). All the parameters of the QSAR models confirmed their reliability and predictability which can be used in the design of new and high selectivity *hu*AChE inhibitors.

From the contour maps (Figure 4), the van der Waals plot (Figure 4a) shows green and yellow contours indicating regions favoring bulky and lighter groups respectively. The mostly yellow colored contours surrounding the most selective molecule **5a** suggests that steric bulk in general is not favorable for *hu*AChE selectivity. Higher selectivity of compounds **5a**, **5i** and **5l** supports this finding.

The electrostatic plot (Figure 4B) shows red and blue contours indicating regions favoring electronegative and electropositive groups respectively. Red colored contours can be seen surrounding the central part of the most selective molecule **5a** indicating that electronegative substituents in the central part of the molecule will be favorable for *hu*AChE selectivity. Both ends of the compound **5a** are surrounded by blue contours, suggesting that these parts can be substituted by electropositive groups for better *hu*AChE selectivity.

3.7 | ADMET analysis

In general, the coumarin derivatives showed good absorption and medium blood-brain barrier penetration. All compounds were predicted to be water soluble. Hepatotoxicity, which is the key problem that limits clinical use of tacrine, was not defined in all synthesized compounds.

4 | EXPERIMENTAL

4.1 | Chemistry

The synthesis pathway of the coumarin derivatives (**5a–p**) is illustrated in Scheme 1. Derivatives of 2-(2-oxo-2*H*-chromen-4-yl)acetic acid (**2a** and **2b**) were prepared via Pechmann condensation between 3-acetone dicarboxylic acid and the corresponding phenol. Isoindoline-1,3-dione derivatives of 1-benzylpiperazine or 1-(3-substituted)-benzylpiperazine (**3a–h**) were synthesized as described in our previous work.[19] Amines **4a–h** were obtained from the treatment of the isoindoline-1,3-diones (**3a–h**) with hydrazine hydrate in ethanol at 80°C.[35] Coupling of the 2-(2-oxo-2*H*-chromen-4-yl)acetic acid (**2a** and **2b**) with amines **4a–h** was performed using coupling reagents [30,36] to yield the amides **5a–p**. Structures of synthesized compounds were determined by IR, ^{1}H-NMR, ^{13}C-NMR and high resolution mass spectrometry.

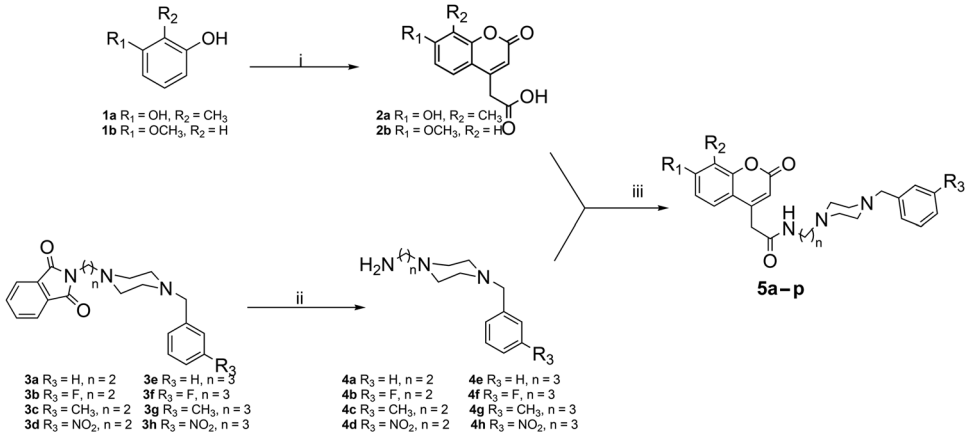

SCHEME 1 Synthesis of the coumarin derivatives. (i) 1,3-Acetone-dicarboxylic acid, H_2SO_4, MeOH; (ii) hydrazine hydrate, EtOH, 80°C; (iii) a. DCC, DMAP, DIEA, CH_2Cl_2, room temperature; b. EDCI, DMAP, DIEA,DMF, room temperature, c. HATU, DIEA, NMP, room temperature

The InChI codes of the investigated compounds together with some biological activity data are provided as Supporting Information.

4.2 | Biological assays

4.2.1 | Cholinesterase inhibition assay

The 2-(2-oxo-2*H*-chromen-4-yl)acetamides were evaluated with the Ellman's method [37] using AChE from humans (*hu*AChE) and human BChE (*hu*BChE). Donepezil, tacrine, and galantamine were used as positive controls. Experimental protocol was as follows: 125 µl of 3 mM 5,5-disthiobis(2-nitrobenzoic acid; DTNB); 25 µl of 1.5 mM acetylthiocholine iodide (ACTI); 1.5 mM butylthiocholine iodide (BuTI) were used for the butylcholinesterase inhibitory assay. A total of 50 µl of 50 mM Tris-HCl buffer pH 8.0; and 25 µl of sample dissolved in ethanol were added to the 96-well microplate followed by 25 µl of AChE enzyme. The absorbance was then measured at 405 nm every 11 seconds for 2 minutes using a microplate reader. A total of 50% inhibition of the AChE and BChE activity (IC_{50}) studies using nine concentrations of compounds **5a–p** (from 0.000398 to 1000 µM) were performed, and the obtained data were analyzed using the Software Prism. Each sample was analyzed in triplicate ($n = 3$).

4.2.2 | Kinetic study

Compound **5a** was selected for the kinetic study because of its highest potency in this series. The velocities of the reaction in the presence and absence of the inhibitor were measured by the spectrophotometric method as described above. Three concentrations of the inhibitor, 0, 10, and 25 µl, were chosen for the assay. For each concentration of the inhibitor, the concentration of the substrate ACTI was varied from 10 to 125 µM. The mode of inhibition of the compound **5a** was evaluated by a global nonlinear regression fit using the kinetic inhibition analysis mode of the GraphPad Prism software and the result was displayed in a Lineweaver-Burk plot.

4.2.3 | Linoleic acid peroxidation inhibition assay

Anti-linoleic acid peroxidation activity was measured by the method of Sekiwa et al.[38] Briefly, the tested compound (final concentration 100 µg/ml) was added to a 2.5% linoleic acid solution, 50 mM phosphate buffer (pH 7.0), and purified water in a screw-cap vial. A solution without the sample was used as a control. BHT was used as the reference compound. Each sample was analyzed in duplicate. Each vial was kept in darkness at 45°C for 20 days and measured every 5 days. The hydroperoxide and aldehyde produced from linoleic acid were determined by the thiocyanate and thiobarbituric acid (TBA) methods, respectively. Sample solutions after the first day and last day of incubation were each subjected to the TBA method. The reaction mixture was added with 20% trichloroacetic acid and 0.67% TBA/99.5% ethanol and the mixture heated in a boiling-water bath for 10 min. The generated TBA reactive substances were measured by their absorbance at 532 nm.

4.2.4 | In vitro cytotoxicity assay

The cytotoxicity assay of the coumarins against HEK-293 cells was measured using a sulforhodamine B (SRB) assay.[39] The cells were cultured in Dulbecco's modified Eagle's medium supplemented with 10% fetal bovine serum (Gibco, Paisley, UK) and grown at 37°C in a humid atmosphere containing 5% CO_2. Cells (5×10^3cells/well) were seeded in a 96-well plate and incubated at 37°C, 5% CO_2 for 24 hr. The cells were then treated with or without various concentrations (0, 3.125, 6.25, 12.5, 25, 50, and 100 µM) of each compound for 48 hours. After an incubation period, 40% (w/v) trichloroacetic acid (TCA) was added to the cells and the cells were then incubated at 4°C for 1 hr. The medium was removed and the cells were rinsed with slow running tap water. A total of 0.4% (w/v) SRB solution (100 µl) was added to each well and the cells were incubated for 1 hr at room temperature. The SRB solution was removed and then the cells were washed three times with 1% (v/v) acetic acid and they were allowed to dry at room temperature. The protein-bound dye was dissolved with 10 mM Tris base solution and the absorbance was measured at 492 nm using a microplate reader.

4.3 | Molecular docking and molecular dynamics simulations

The initial structures of recombinant human acetylcholinesterase (*hu*AChE) (PDB ID: 4EY7) and human butyrylcholinesterase (*hu*BChE) (PDB ID:4BDS) were retrieved from the protein data bank and minimized using AMBER software. The protonation state of ionizable protein side chains was assigned at pH 7. The structures of inhibitors were optimized using the density functional theory. Molecular docking was performed using AutoDock Vina where the binding site was covered the PAS and CAS of the enzyme. The box dimension of 30 × 30 × 30 Å was allowed for the ligand to explore for the best binding interaction. The catalytic binding sites (CAS) include three catalytic triads (*hu*AChE: Ser203, Glu334 and His447 and *hu*BChE: Ser198, Glu325, and His438) and the peripheral site, PAS (*hu*AChE: Tyr72, Asp74, Tyr124, Trp286 and *hu*BChE: Tyr341 and Asp70 and Tyr332). The best docked pose in agreement with the X-ray structure with the lowest binding affinity was selected and its respective residue binding interaction energy was calculated. Selected complexes were further investigated with MDs using AMBER14 force field for 20 ns. More method details are included in the Supporting Information.

4.3.1 | 3D QSAR modeling

A data set comprising 16 compounds with their *hu*AChE and *hu*BChE IC_{50} (nM) data was used for the development of the atom-based 3D QSAR model for *hu*AChE selectivity. The *hu*AChE IC_{50} and *hu*BChE IC_{50} values were first transformed to the respective pIC_{50}

(–log IC_{50}). The *hu*AChE selectivity ($SI = pIC_{50huAChE} - pIC_{50huBChE}$) was then calculated and used as the dependent variable for the 3D QSAR modeling. The 3D QSAR studies were performed using Discovery Studio 3.1. The ligands were pre-aligned using the substructure based molecular overlay method and placed in a 3D grid space. The grid spacing was 1.5 Å. The energy potentials on every grid point were then calculated using a CHARMm force field which used the electrostatic potential and the van der Waals potential and treated them as separate terms. A + 1e point charge is used as the electrostatic potential probe and distance-dependent dielectric constant is used to mimic the solvation effect. For the van der Waals potential a carbon atom with a 1.73 Å radius was used as a probe. The energy grid potentials can be used as independent variables to create partial least-squares. Validation was performed using leave-one-out cross validation method (five folds). The 3D QSAR was evaluated by using r^2 and cross validated r^2.

4.3.2 | ADMET analysis

Drug-likeness of the designed compounds was predicted using the Discovery Studio 2.5 program.

ACKNOWLEDGMENTS

The authors would like to thank Prince of Songkla University (grant no. PHA570404S) and University of Malaya (Faculty Research Grant: GPF063B-2018) for financial support. The authors would like to thank Miss Maria Mullet for providing linguistic proofreading for the manuscript.

CONFLICT OF INTERESTS

The authors declare that there are no conflict of interests.

ORCID

Luelak Lomlim http://orcid.org/0000-0003-1229-2189

REFERENCES

[1] Alzheimer's Association, *J. Alzheimer's Assoc.* **2017**, *13*(4), 325.
[2] J. L. Sussman, M. Harel, F. Frolow et al., *Science* **1991**, *253*, 872.
[3] R. M. Lane, S. G. Potkin, A. Enz, *Int. J. Neuropsychopharmacol.* **2006**, *9*, 101.
[4] A. N. Cokugras, *J. Biochem.* **2003**, *28*, 54.
[5] U. Holzgrabe, P. Kapková, V. Alptüzün, J. Scheiber, E. Kugelmann, *Expert Opin. Ther. Targets* **2007**, *11*, 161.
[6] G. Kryger, I. Silman, J. L. Sussman, *Structure* **2003**, *7*, 297.
[7] D. Muñoz-Torrero, P. Camps, *Curr. Med. Chem.* **2006**, *13*, 399.
[8] L. Piazzi, A. Rampa, A. Bisi et al., *J. Med. Chem.* **2003**, *46*, 2279.
[9] X. Zhou, X. B. Wang, T. Wang, L. Y. Kong, *Bioorg. Med. Chem.* **2008**, *16*, 8011.
[10] B. Tasso, M. Catto, O. Nicolotti et al., *Eur. J. Med. Chem.* **2011**, *46*, 2170.
[11] M. Alipour, M. Khoobi, A. Foroumadi et al., *Bioorg. Med. Chem.* **2012**, *20*, 7214.
[12] M. Catto, L. Pisani, F. Leonetti et al., *Bioorg. Med. Chem.* **2013**, *21*, 146.
[13] J. I. da Silva, M. C. de Moraes, L. C. C. Vieira, A. G. Corrêa, Q. B. Cass, C. L. Cardoso, *J. Pharm. Biomed. Anal.* **2013**, *73*, 44.
[14] S. F. Razavi, M. Khoobi, H. Nadri et al., *Eur. J. Med. Chem.* **2013**, *64*, 252.
[15] S. O. Nam, D. H. Park, Y. H. Lee, J. H. Ryu, Y. S. Lee, *Bioorg. Med. Chem.* **2014**, *22*, 1262.
[16] J. B. Shaik, B. K. Palaka, M. Penumala et al., *Eur. J. Med. Chem.* **2015**, *107*, 219.
[17] S. Ghanei-Nasab, M. Khoobi, F. Hadizadeh et al., *Eur. J. Med. Chem.* **2016**, *121*, 40.
[18] L. G. de Souza, M. N. Renn, J. D. Figueroa-Villar, *Chem. Biol. Interact.* **2016**, *254*, 11.
[19] J. B. Shaik, B. K. Palaka, M. P. et al., *Eur. J. Med. Chem.* **2016**, *107*, 219.
[20] F. Sonmez, B. Z. Zengin kurt, I. Gazioglu et al., *J. Enzyme Inhib. Med. Chem.* **2017**, *32*, 285.
[21] M. Alipour, M. Khoobi, H. Nadri et al., *Arch. Pharm. Chem. Life Sci.* **2013**, *346*, 577.
[22] M. Alipour, M. Khoobi, A. Moradi et al., *Eur. J. Med. Chem.* **2014**, *82*, 536.
[23] D. Yao, J. Wang, G. Wang et al., *Bioorg. Chem.* **2016**, *68*, 112.
[24] L. Pisani, R. Farina, M. Catto et al., *J. Med. Chem.* **2016**, *59*, 6791.
[25] J. Kara, C. Wattanapiromsakul, L. Lomlim, *SDU Res. J.* **2013**, *6*, 141.
[26] W. Si, T. Zhang, L. Zhang et al., *Bioorg. Med. Chem. Lett.* **2016**, *26*, 2380.
[27] D. Panek, A. W. Ckowska, T. Wichur et al., *Eur. J. Med. Chem.* **2017**, *125*, 676.
[28] M. A. Ansari, S. W. Scheff, *J. Neuropathol. Exp. Neurol.* **2010**, *69*, 155.
[29] W. -J. Huang, X. Zhang, W. -W. Chen, *Biomed. Rep.* **2016**, *4*, 519.
[30] S. Sharma, S. Verma, M. Kapoor, A. Saini, B. Nehru, *Neurol. Res.* **2016**, *38*, 838.
[31] C. Cheignon, M. Tomas, D. Bonnefont-Rousselot, P. Faller, C. Hureau, F. Collin, *Redox Biol.* **2018**, *14*, 450.
[32] I. Kostova, S. Bhatia, P. Grigorov et al., *Curr. Med. Chem.* **2011**, *18*, 3929.
[33] G. B. Bubols, R. Vianna Dda, A. Medina-Remon et al., *Mini Rev. Med. Chem.* **2013**, *13*, 318.
[34] Y. Al-Majedy, A. Al-Amiery, A. A. Kadhum, A. Bakar Mohamad, *Sys. Rev. Pharm.* **2017**, *8*, 24.
[35] S. N. Haydar, C. Ghiron, L. Bettinetti et al., *Bioorg. Med. Chem.* **2009**, *17*, 5247.
[36] L. Lomlim, J. Einsiedel, F. W. Heinemann, K. Meyer, P. Gmeiner, *J. Org. Chem.* **2008**, *73*, 3608.
[37] G. L. Ellman, K. D. Courtney, J. R. V. Andres, V. Featherstone, M. Robert, *Biochem. Pharmacol.* **1961**, *7*, 88.
[38] Y. Sekiwa, K. Kubota, A. Kobayashi, *J. Agric. Food. Chem.* **2000**, *48*, 373.
[39] P. Skehan, R. Storeng, D. Scudiero et al., *J. Natl. Cancer Inst.* **1990**, *82*, 1107.

SUPPORTING INFORMATION

Additional supporting information may be found online in the Supporting Information section at the end of the article.

How to cite this article: Kara J, Suwanhom P, Wattanapiromsakul C, et al. Synthesis of 2-(2-oxo-2*H*-chromen-4-yl)acetamides as potent acetylcholinesterase inhibitors and molecular insights into binding interactions. *Arch. Pharm. Chem. Life Sci.* 2019;e1800310. https://doi.org/10.1002/ardp.201800310